PDE-BASED NON-RIGID REGISTRATION OF BREAST SURFACES

By

Rowena E. Ong

Thesis

Submitted to the Faculty of the

Graduate School of Vanderbilt University

in partial fulfillment of the requirements

for the degree of

MASTER OF SCIENCE

in

Biomedical Engineering

December, 2007

Nashville, Tennessee

Approved:

Professor Michael I. Miga

Professor Robert L. Galloway

ACKNOWLEDGEMENTS

I would like to thank my advisors Dr. Michael Miga and Dr. Bob Galloway for their guidance and Jao Ou for his advice in phantom construction and algorithmic development. I am grateful to the members of the BML and SNARL labs for their support and friendship and to the Vanderbilt Medical Center CT department for their generosity in scanning our phantoms. I would also like to thank Dr. Thomas Yankeelov for his help obtaining the clinical data and Dr. John Boone (University of California-Davis Medical Center, Dept. of Radiology) for the human breast CT data set. This work was supported by the Whitaker Foundation Young Investigator Award.

TABLE OF CONTENTS

LIST OF TABLES

Table Page

LIST OF FIGURES

LIST OF ABBREVIATIONS AND NOMENCLATURE

Abbreviation	Full Name
1. TPS	Thin-plate spline
2. MIE	Modality-independent elastography
3. FEM	Finite element method
4. SCP	Symmetric closest point
5. RPM	Robust point matching
6. TRE	Target registration error
7. PDE	Partial differential equation
8. MR	Magnetic resonance
9. CT	Computed tomography
10. w/v	Weight per volume
11. ∇	Gradient operator
12. $\cdot$	Divergence operator

CHAPTER 1

INTRODUCTION

1.1 Motivation

As breast cancer is estimated to kill over 40,000 women and be diagnosed in more than 178,000 in 2007 (American Cancer Society, 2007), the detection and treatment of breast cancer is an important area of scientific research. Many novel techniques to aid in tumor detection are being developed that exploit the difference in physical properties between healthy and cancerous tissue. Some of these techniques measure the optical, electrical, or elastic properties of tissue, such as near-infrared tomography (Brooksby, et al, 2003), electrical impedance tomography (Bayford 2006), ultrasound elastography (Pellot-Barakat 2006), and magnetic resonance elastography (Greenleaf, et al, 2003). One recently proposed approach utilizes a non-rigid image registration and inverse problem formulation to calculate the spatially varying elastic properties of tissue. This method is called modality-independent elastography (MIE) (Miga, 2003), (Washington & Miga, 2004), because it can be applied to any imaging modality.

MIE is a reconstruction algorithm for elasticity imaging that can be used for detecting breast tumors. It involves imaging a pendent breast before and after a compression and using these images to reconstruct the elastic properties of the tissue. The elastic properties are recovered by solving an inverse model of soft-tissue deformation using nonlinear optimization and standard measures of image similarity. Unique to MIE is its ability to utilize images from any modality such as MRI or CT, as well as its usage of image similarity measures that make direct displacement measurements unnecessary.

One requirement of MIE is a semi-automated method of registering the pendent breast surfaces before and after compression, as the surface point correspondences are needed to specify the boundary conditions for the elasticity model. Because the breast is composed of soft tissue that deforms non-rigidly, standard rigid registration methods cannot be applied. The goal of this work is to develop and validate a non-rigid registration method that can semi-automatically

register breast surfaces before and after compression. These non-rigid registration methods not only have the potential to be used in MIE, but also in other applications that require breast surface registration.

1.2 Previous work

Previous work in non-rigid registration has been broadly categorized as being feature-based or intensity-based. Feature-based methods use only the geometric information extracted from an image, such as the polygonal mesh extracted from a segmented image. In contrast, intensity-based methods utilize the intensities in the image volume, sometimes in addition to the geometric information, to register two images. Guo (2006) published a review of both these non-rigid and rigid registration techniques and their application to breast images.

One type of feature-based registration involves the use of splines to interpolate the displacements between tracked control points. Polynomial splines, B-splines, and thin-plate splines (TPS) are three commonly used splines. Davis (1997) developed the elastic body spline, a new type of spline that was derived from the Navier equations describing a homogenous, isotropic, elastic material. However, the difficulty with using any type of spline is determining accurate displacements at the control points: the displacements must either be tracked with fiducial markers or estimated using another method. Thirion (1996) used curvature measures to estimate the displacements at certain locations that could be then interpolated using a spline.

Another type of non-rigid registration involves using the finite element method (FEM) to model an object's deformation. Roose (2006) modeled the breast tissue as a linear elastic, homogenous tissue, and used FEM solve for the displacements after a deformation. The boundary conditions were determined in a simplistic manner: the Iterative Closest Point (ICP) method (Besl & McKay, 1992) was used to rigidly align the undeformed and deformed surfaces, and the displacements at the surface were found by projecting the points on one surface to the other along the normal direction.

Other feature-based methods include the symmetric closest point (SCP) (Papademetris, 2002) and robust point matching (RPM) (Chui, 2003) methods. Both these methods use a

heuristic or probability at each surface point and its neighbors to find correspondence. Another method developed by Dinh (2002) uses implicit functions to solve for a transformation spanning space and time that describes how a source object morphs into a target object.

Much work has been done to develop intensity-based registration methods as well. Rueckert (1999) developed a method that used optimization to find the deformation that best maximized image similarity and preserved smoothness. The deformation was described using B-splines, and the cost function contained a normalized mutual information term and a term to preserve smoothness. A similar volume-preserving optimization method was developed by Rohfing (2003). Tanner (2007) conducted a validation study and compared Rueckert and Rohfing's methods. In this study, a biomechanical model of breast tissue was used to simulate breast deformation, and the resulting deformed and undeformed image volumes were registered, allowing the target registration error (TRE) to be calculated. Similar optical flow (Froh, 2006) and fluid flow (Crum, 2005) techniques have been also developed for breast image registration.

Although much focus recently has been on intensity-based methods, the disadvantage of these methods, like all involving optimizations, is that they require a good initialization, may fall into local minima, and may be computationally expensive. In all these methods, the central problem remains: to find accurate displacements at certain points so that they can be interpolated to the rest of the breast volume or surface.

In this thesis, a feature-based, semi-automated method is presented that uses the Laplace or diffusion equations to non-rigidly register deformed breast surfaces. This method was compared to a standard thin-plate spline interpolation method (Goshtasby, 1988) and validated using biomechanical simulations and realistic breast phantoms.

CHAPTER 2

METHODOLOGY

2.1 PDE-based registration

A major investigative task of this work was to evaluate whether the energy distributions modeled by a partial differential equation (PDE) over an undeformed (*source*) surface and a deformed (*target*) surface can be used to find the correspondence between the two surfaces. In this method, a PDE was independently solved over the source and target meshes using FEM. Two different PDEs, the Laplace and the diffusion equation, were evaluated in this work to see whether one yielded more accurate registrations. Laplace's equation is most commonly used to describe potential flow problems such as in thermal, fluid, and electrostatic systems and is given by

$$\nabla \cdot (\sigma \nabla \Phi) = 0 \tag{1}$$

where Φ represents the potential and σ describes the spatially varying conductivity. The diffusion equation which allows a time-varying potential is given by

$$\frac{d\Phi}{dx} - \nabla \cdot (\alpha \nabla \Phi) \tag{2}$$

where Φ represents the potential and α is the diffusion coefficient. Let Φ_{source} refer to the solution to the Laplace or diffusion equation over the source surface, and let Φ_{target} refer to the solution over the target. The basic premise is that Φ_{source} and Φ_{target}, the potential fields distributed over the source and target surfaces as calculated by the Laplace or diffusion equation, will provide information about the correspondence between the source and target surfaces.

To solve the Laplace equation (1), a Galerkin weighting scheme using Lagrange polynomials was applied, and Dirichlet (type 1) boundary conditions were set to simulate potential flow from an inflow source at the nipple to an outflow sink at the chest wall. Specifically, nodes in the nipple and chest wall area were given boundary potential values of 1 and 0, respectively, and the conductivity σ was set to unity.

The diffusion equation (2) was solved in a similar manner: Galerkin weighting using Lagrange polynomials was applied to solve for the spatial component of the PDE, and a fully explicit forward Euler scheme was used to solve for the temporal component. A pure Neumann (type 2) no-flux boundary condition was prescribed at the chest wall, and the potential field was allowed to propagate from a source at the nipple. The diffusion coefficient α was set to unity. In this calculation, time-stepping was stopped once the potential field reached the chest wall.

After the Laplace or diffusion equation was solved over the source and target surfaces, the solutions Φ_{source} and Φ_{target} were used to establish correspondence between the source and target nodes. This involved two distinct processes: finding point correspondence between isocontours of Φ_{source} and Φ_{target} and interpolating the displacements at these isocontour points to all nodes in the mesh. In the first step, isocontours were extracted from Φ_{source} and Φ_{target} for a set of selected isovalues. The correspondence between the source and target isocontour points was determined by aligning the contours by their centroids and using the symmetric closest point (SCP) algorithm (see Figure 3-4 for SCP description). In the second step, the displacement vectors at the source isocontours points were interpolated to all source nodes using a thin-plate spline. The final correspondence was found by adding these displacements to the source nodes to get the location of the corresponding point on the target surface.

The method can be summarized in the following steps (Figure 1, 2):

1. Obtain the undeformed source mesh and deformed target mesh that define a breast surface before and after deformation.
2. Assign boundary conditions at nipple and/or chest wall nodes
3. Solve the PDE (diffusion or Laplace) over the source and target meshes using FEM.
4. Extract isocontours on the source and target surfaces.
5. Determine point correspondence between source and target isocontours using SCP (Figure 3-4).
6. Interpolate displacements at source isocontours to all source nodes.

This method was implemented using Matlab.

1. Obtain the undeformed source (left) and deformed target mesh (right) that define a breast surface before and after deformation.

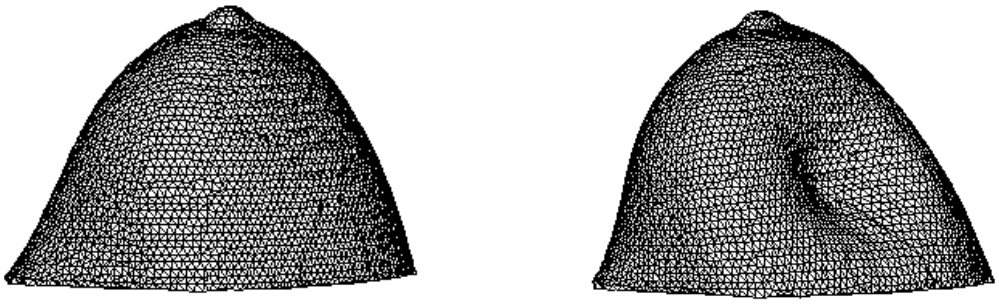

2. Assign boundary conditions at the nipple and chest wall nodes on the source (left) and target (right) meshes. To solve the Laplace equation, assign type 1 boundary conditions at nipple nodes (Φ=1, assigned at the red nodes in the illustration below) and at chest wall nodes (Φ=0, blue nodes). To solve the diffusion equation, assign type 1 boundary conditions at nipple (Φ=1, red nodes) and no-flux conditions at chest wall nodes ($d\Phi/d\mathbf{X} = 0$).

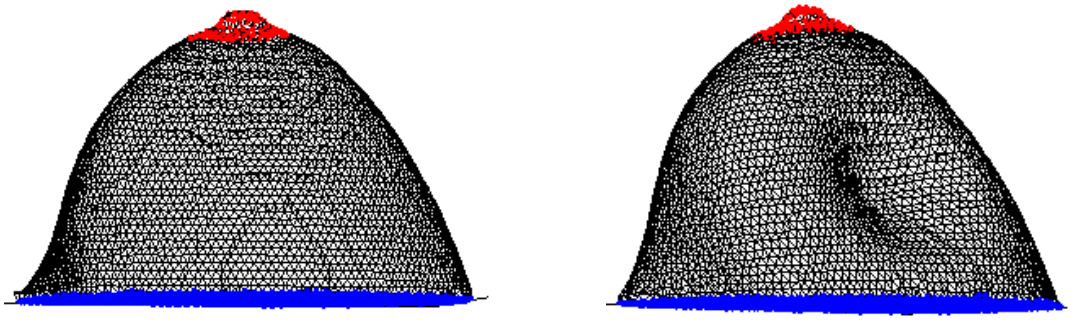

3. Solve the Laplace or diffusion equations over the source (left) and target (right) meshes using FEM. The solutions to the Laplace or diffusion equation Φ_{source} and Φ_{target} are given by an array of scalars describing the potential at each surface node (indicated by the shading in the figures below)

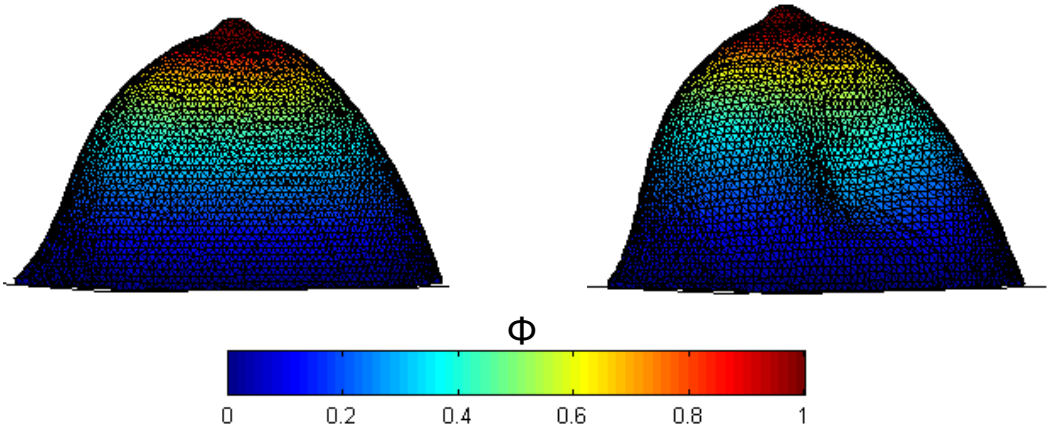

Figure 1. Summary of the PDE-based registration method (steps 1-3).

4. Extract isocontours on the source (left) and target (right) surfaces.

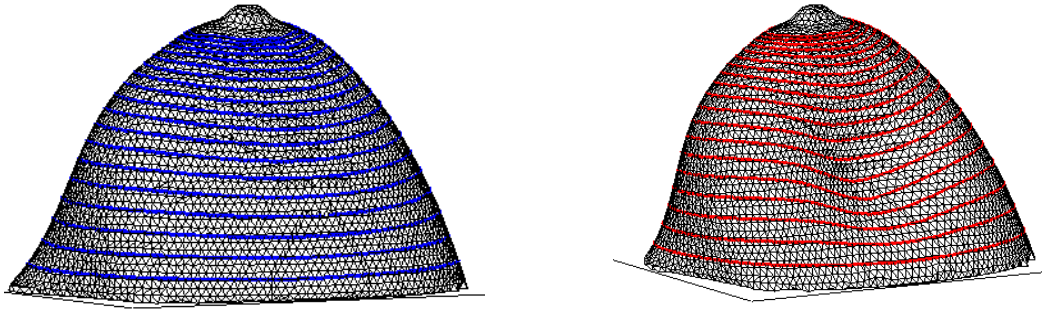

5. Determine point correspondence between source and target isocontours using SCP method (Figure 3-4). For each isovalue, the SCP method will return a mapping between the source isocontour (blue) and target isocontour (red) points. The vectors describing the displacement (black dotted lines) between the source and target isocontour points can then be calculated by a simple subtraction.

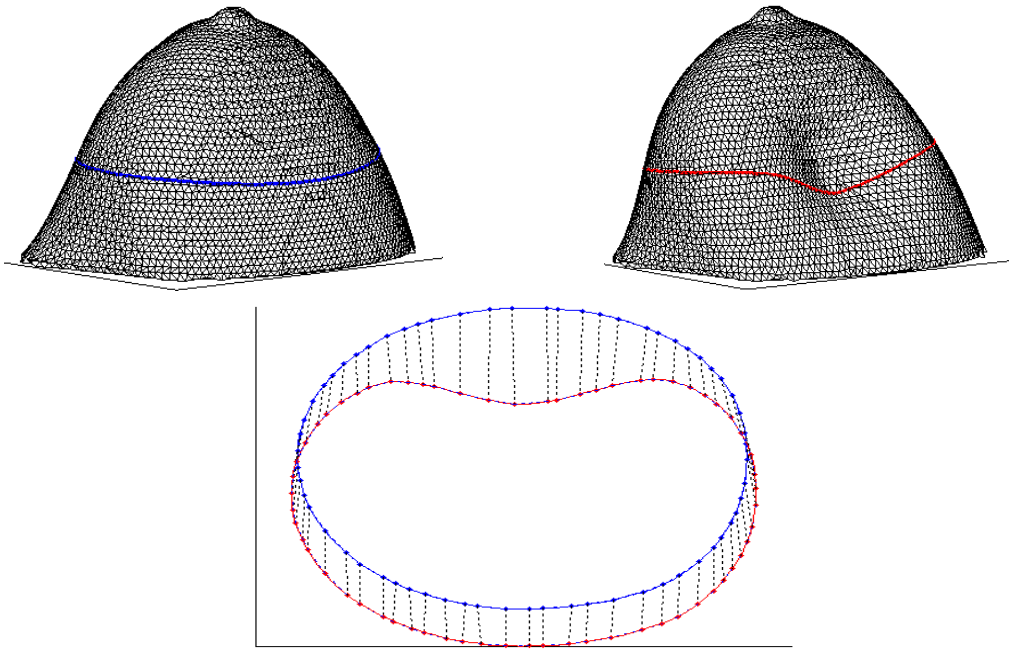

6. Interpolate displacements from source isocontour points (blue nodes) to all source nodes (black nodes). The registered target surface can then be reconstructed by adding the displacement vectors to the source nodes.

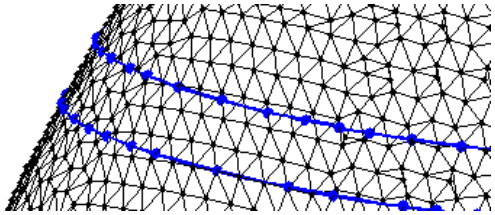

Figure 2. Summary of the PDE-based registration method (steps 4-6).

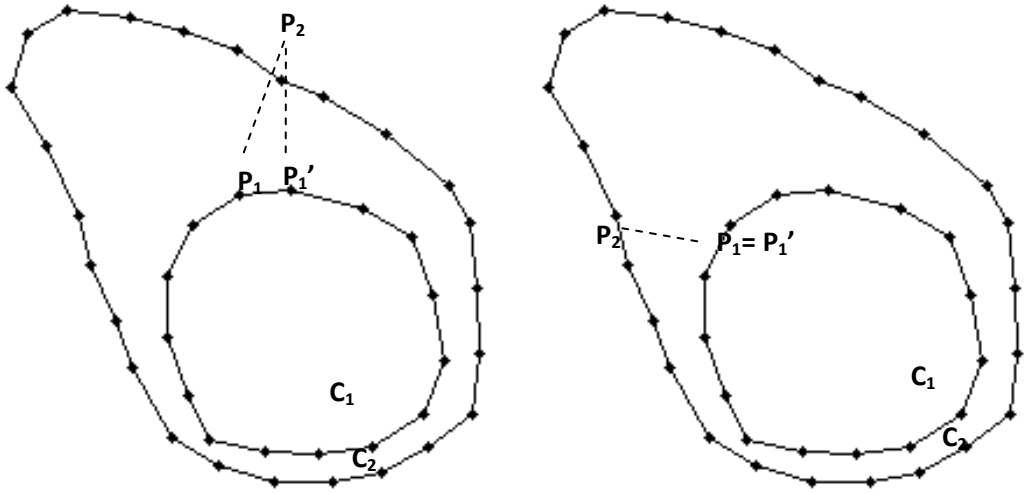

Figure 3. The first step in the symmetric closest point algorithm is to find the set of symmetric closest points: for each point P_1 on contour C_1, find the nearest neighbor p2 on contour c2. Then for each point P_2, find the nearest neighbor P_1' on C_1. If P_1=P_1', then P_1 and P_2 are considered symmetric closest points. In the left illustration above, P_1 and P_2 are not symmetric closest points; in the right illustration, P_1 and P_2 are symmetric closest points.

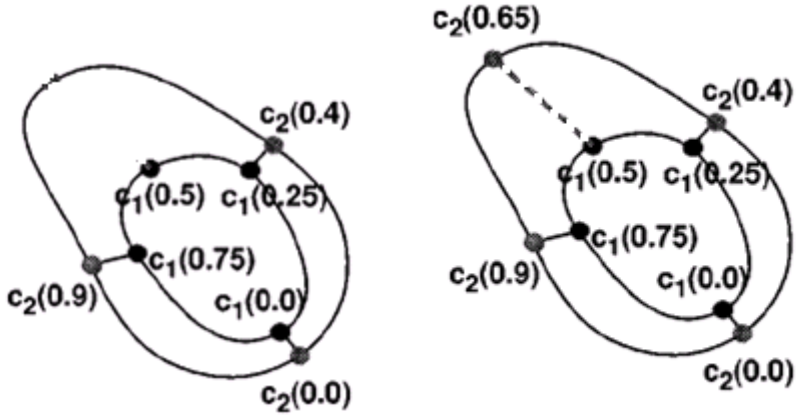

Figure 4. Once the set of symmetric closest points have been found, the second step of the symmetric closest point method is to parameterize each contour and interpolate to find correspondence for all points not in the set of symmetric closest points. In the example shown in this figure, points C1(0.0), C1(0.25), and C1(0.75) have symmetric closest points C2(0.0), C2(0.4), and C2(0.9), respectively, while C1(0.5) does not have a symmetric closest point (left illustration). To find the point on c2 that corresponds to point C1(0.5), parameterize contours C1 and C2 by arc length and interpolate to find the point C2(0.65) that matches C1(0.5) (right illustration). (Figure courtesy of Papademetris 2002)

2.2 TPS registration

One advantage of the PDE-based correspondence methods is that they do not explicitly rely on external markers to constrain the matching process. However, when real-world data is acquired, fiducial markers are anticipated to be available. The TPS method involves interpolating the displacements tracked by fiducials to all surface nodes (Goshtasby, 1988), allowing the two surfaces to be registered. The displacement vector at point (x,y,z) in a given direction is described by the following equation:

$$f(x,y,z) = a \cdot x + b \cdot y + c \cdot z + \sum_{i=1}^{N} F_i \cdot r_i^2 \cdot \ln r_i^2 \quad (3)$$

with constraints

$$\sum_{i=0}^{N} F_i = 0$$

$$\sum_{i=0}^{N} X_i F_i - 0$$

$$\sum_{i=0}^{N} Y_i F_i = 0$$

$$\sum_{i=0}^{N} Z_i F_i = 0$$

where

$$r_i^2 = (x - X_i)^2 + (y - Y_i)^2 + (z - Z_i)^2$$

and (Xi, Yi, Zi) are the coordinates of the control points, N is the number of control points, and ***a***, ***b***, ***c***, and ***F*** are constants. The TPS method was implemented in Matlab.

Although there are many different methods for interpolation, including polynomial splines and B-splines, TPS interpolation was chosen in part because it does not require a regular grid, the effects of changing a control point are localized, and it is a standard method that has been successfully used in many non-rigid registration applications.

2.3 Simulation experiments

To perform a controlled evaluation of the PDE-based and TPS registration methods described above, two source surfaces were extracted from an MR and CT image volume of a human breast and registered to deformed target surfaces created by different simulated compressions.

A CT image volume of a human pendant breast (256 x 256 x 130, voxel size 0.6 mm^3, courtesy of the Dept. of Radiology, University of California-Davis) and an MR image volume of a pendant breast from a different patient (256 x 256 x 98, voxel size 1.0 mm^3, using 3D T1-weighted fat-nulling inversion pulse sequence, courtesy of Dr. Thomas Yankeelov, Vanderbilt University) were obtained. Both the CT and MR image volumes were segmented using Analyze 6.0 (Mayo Clinic, Rochester, MN), and two triangular source meshes consisting of 6,313 and 3942 nodes, respectively, were extracted from the segmented volumes.

To create deformed target surfaces, the breast was modeled as linear elastic, Hookean solid, and a three-dimensional compression was simulated using FEM (Figure 5). The nodes along the chest wall were assumed to be fixed, and a Gaussian-shaped stress distribution against the lateral surface of the breast was applied, yielding type 1 and 2 boundary conditions, respectively. These boundary conditions seem to be reasonable given the anatomy of the breast and that the shape of the stress distribution approximates that of an inflating air bladder used to apply compression to the breast in later experiments. However, because exactly how the breast interacts with a compression bladder in a clinical application is unknown, three different simulations were performed assuming slightly different compression properties.

In the first CT simulation, the CT source surface was deformed assuming a circular contact area between the Gaussian-shaped stress field and the breast surface, with a maximum displacement of approximately 33 mm. Similarly, in the second CT simulation the CT source surface was deformed assuming a rectangular contact area and maximum displacement of 13 mm. Finally, in the third MR simulation, the MR source surface was deformed assuming a rectangular contact area and a maximum displacement of 6 mm. The source and target surfaces

deformed by these simulations were then registered using the Laplace, diffusion, and TPS registration methods.

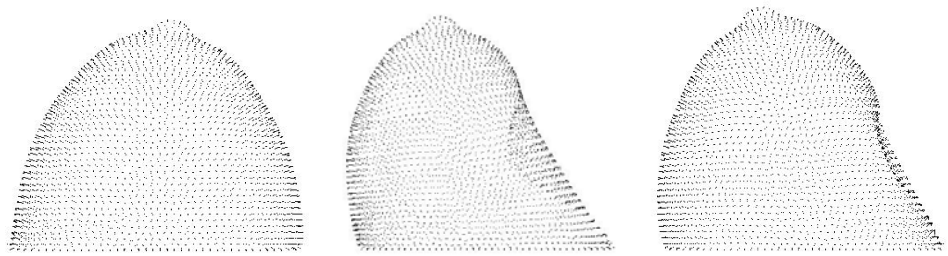

Figure 5. CT breast surfaces used to test registration methods. Undeformed source surface extracted from a CT volume of a human breast (left). Deformed target surface generated by CT simulation 1 (middle, assuming a circular contact area with the simulated compression bladder and max displacement of 33 mm) and CT simulation 2 (right, assuming a rectangular contact area and max displacement of 13 mm).

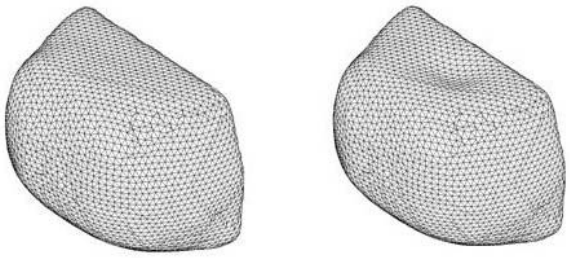

Figure 6. MR breast surfaces used to test registration methods. Undeformed source surface extracted from an MR volume of a human breast (left) and target surface deformed by MR simulation 3 (right).

To assess the accuracy of the registration methods, the target registration error (TRE) was calculated. The TRE measures the error between the correspondence determined by the registration method and the true correspondence (Hajnal, Hill, Hawkes, 2001). In these simulations, the TRE was calculated as the Euclidean distance between the target points determined by the registration and the true target points. Since the true correspondence between the source and target surfaces was known, the TRE was calculated for each source node, and the average and maximum were reported.

Because the accuracy of the TPS registration can vary based on the number and distribution of fiducials used, two different analyses were performed to assess the accuracy and how it is affected by fiducial number and distribution. In both analyses, the mean and maximum TRE were calculated for differing numbers of fiducials; however, the first analysis used a uniform distribution of fiducials while the second analysis used a high number of fiducials in the deformed region (the part of the surface in contact with the simulated inflation bladder) and a lower number over the rest of the surface. In order to account for the variability in TRE due to the arbitrary fiducial locations (chosen using k-means clustering with random seed locations), in both analyses the maximum and mean TRE were averaged over 20 trials.

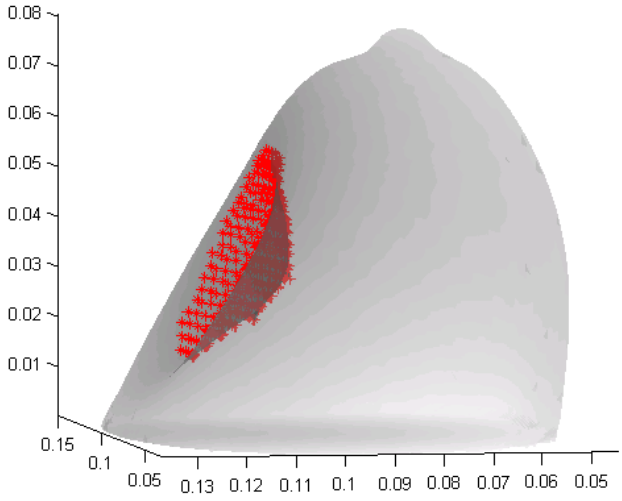

Figure 7. Breast surface with deformed region (the area in contact with the simulated inflation bladder) highlighted in red. Accuracy of TPS registration was tested using a uniform fiducial distribution across the breast surface and a non-uniform distribution with a higher number of fiducials in the deformed region.

2.4 Phantom experiments

A breast phantom was constructed to test the registration methods with real-world data. The phantom was fabricated from an 8% w/v solution of polyvinyl alcohol that was frozen in the upper half of a 2-liter beverage container for 16 hours. After 8 hours of thawing, thirty-four 1-mm

stainless steel ball bearings were implanted directly under the surface of the resulting cryogel to act as fiducials.

The phantom was then imaged inside a custom-built rectangular chamber designed to deliver compression by means of an air bladder placed against the surface of the phantom (Figure 8). CT images (512 x 512 x 174, 0.54 x 0.54 x 1 mm voxel spacing) were acquired with the phantom at three different states of mechanical deformation (undeformed, 50% of maximum bladder pressure, and full inflation). Triangular surface meshes were obtained by semi-automatic segmentation of the image volumes using the surface extraction tools in ANALYZE 6.0 (Mayo Clinic, Rochester, MN), and the coordinates of the fiducial centroids were localized. These meshes contained approximately 8127, 6777, and 8260 nodes, respectively. The Laplace, diffusion, and TPS methods were then used to register the phantom surface meshes, and the TRE at the fiducial targets was calculated.

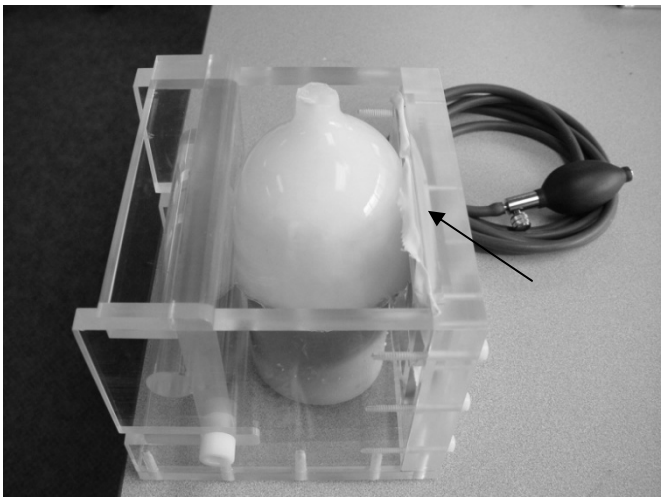

Figure 8. Experimental system for applying compression to breast phantom. A polyvinyl alcohol cryogel is placed within a Plexiglas chamber with its surfaces held in place against the walls. Compression is delivered through an air bladder (arrow) inflated manually through a bulb adapted from a standard sphygmomanometer.

For the TPS method, 33 of the fiducials were used in the interpolation and the remaining fiducial was reserved for calculating the TRE. To assess the error over the entire surface, the

TPS registration was repeated, each time using a different fiducial to calculate the TRE. The TRE over all trials was then averaged, yielding a TRE estimate over the entire surface, rather than just at one target fiducial.

2.5 Clinical experiment

In addition to the breast simulation and phantom, the PDE-based and TPS registration methods were tested on clinical data to test their feasibility in a clinical application. MR image volumes (192x192x160, 1x1x1 mm voxel spacing, T1-weighted) of a subject's uncompressed and compressed pendent breast were obtained using a custom-built device containing a MR coil and compression chamber (Figure 9). Similar to the compression chamber described in the phantom experiments, the compression in this device is delivered through a manually inflated air bladder. The image volumes obtained were segmented semi-automatically using ANALYZE 6.0, and triangular surface meshes were extracted. The PDE-based methods were used to register the undeformed source and deformed target surfaces. As no fiducial markers were available for this dataset, the TPS registration method could not be used and the TRE could not be calculated.

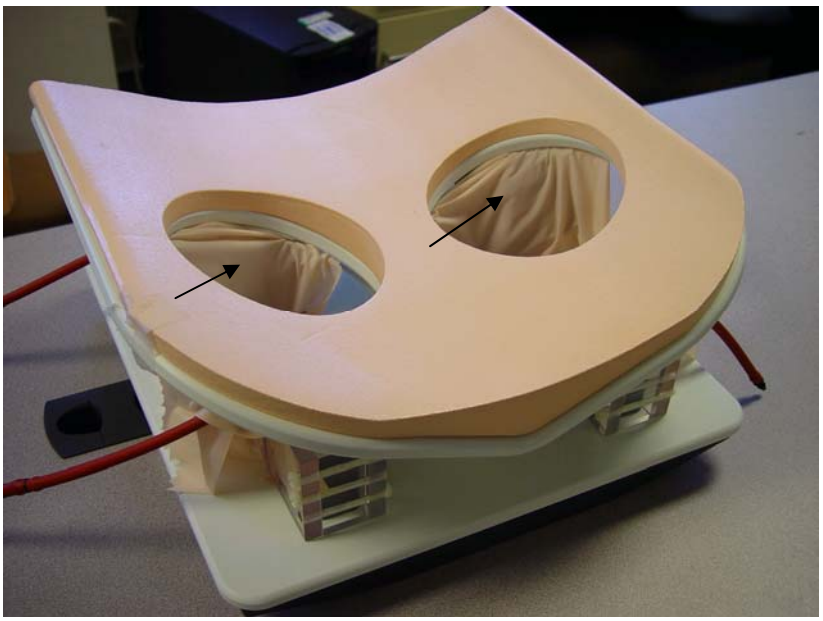

Figure 9. Breast MR coil with manually inflated air bladders (indicated by arrows) used to obtain clinical data for MIE elasticity reconstructions.

2.6 MIE reconstruction

In addition to assessing the accuracy of the Laplace, diffusion, and TPS registrations, an additional experiment was conducted to evaluate the efficacy of their results in the context of a real-world application. MIE is one such application that requires a known correspondence between the source and target surface nodes, which is used as the boundary condition to drive the three-dimensional elasticity reconstruction. As the MIE elasticity reconstruction is very sensitive to the accuracy of the boundary conditions, the goal of this experiment was to see how accurately MIE could reconstruct simulated tissue elasticities given boundary conditions specified by the Laplace, diffusion, and TPS registrations.

In this experiment, MIE elasticity reconstructions were performed on the breast data set deformed by CT simulation 1 (described in Section 2.3). In the reconstruction, the breast was specified as a homogenous tissue containing a spherical tumor that had an elasticity six times stiffer than the surrounding tissue. The elastic contrast ratio, i.e. the ratio of the tumor elasticity to the surrounding tissue elasticity, was then reconstructed using MIE, given boundary conditions established by Laplace, diffusion, and TPS registrations. The accuracy of each reconstruction was assessed by comparing the reconstructed elastic contrast ratio to the simulated contrast ratio.

CHAPTER 3

RESULTS

3.1 Simulation experiments

The Laplace and diffusion methods were used to register the breast surfaces deformed by the three simulated compressions described in section 2.3. For each simulation, the accuracy of the Laplace and diffusion methods was assessed by calculating the TRE at each node (Figure 10). For comparison, the TPS registration was also performed on the three simulation datasets, and the TRE calculated for differing numbers of fiducials, placed in uniform (Figure 11) and nonuniform (Figure 12) fiducial distributions.

The results (Table 2) indicated that the TPS registration method performed more accurately overall than the Laplace and diffusion methods. The distribution of error varied based on breast geometry, method of simulating compression, and registration error.

The results of the TPS registrations indicate that when a uniform fiducial distribution is used, the error decreases as the number of fiducials is increased. However, increasing the fiducial number over about 40 does not seem to result in a significant error reduction (Figure 11). To test the effects of a non-uniform fiducial distribution, in which the number of fiducials per unit area is higher in region in contact with the simulated compression bladder, the number of fiducials in the deformed region was kept constant at 12, and the number outside the deformed region was varied. The results indicate that the error does not decrease as the number of fiducials outside the contact region is increased (Figure 12). In other words, the same amount of error can be obtained using a smaller number of fiducials, as long as more fiducials are placed in the region in contact with the simulated compression bladder.

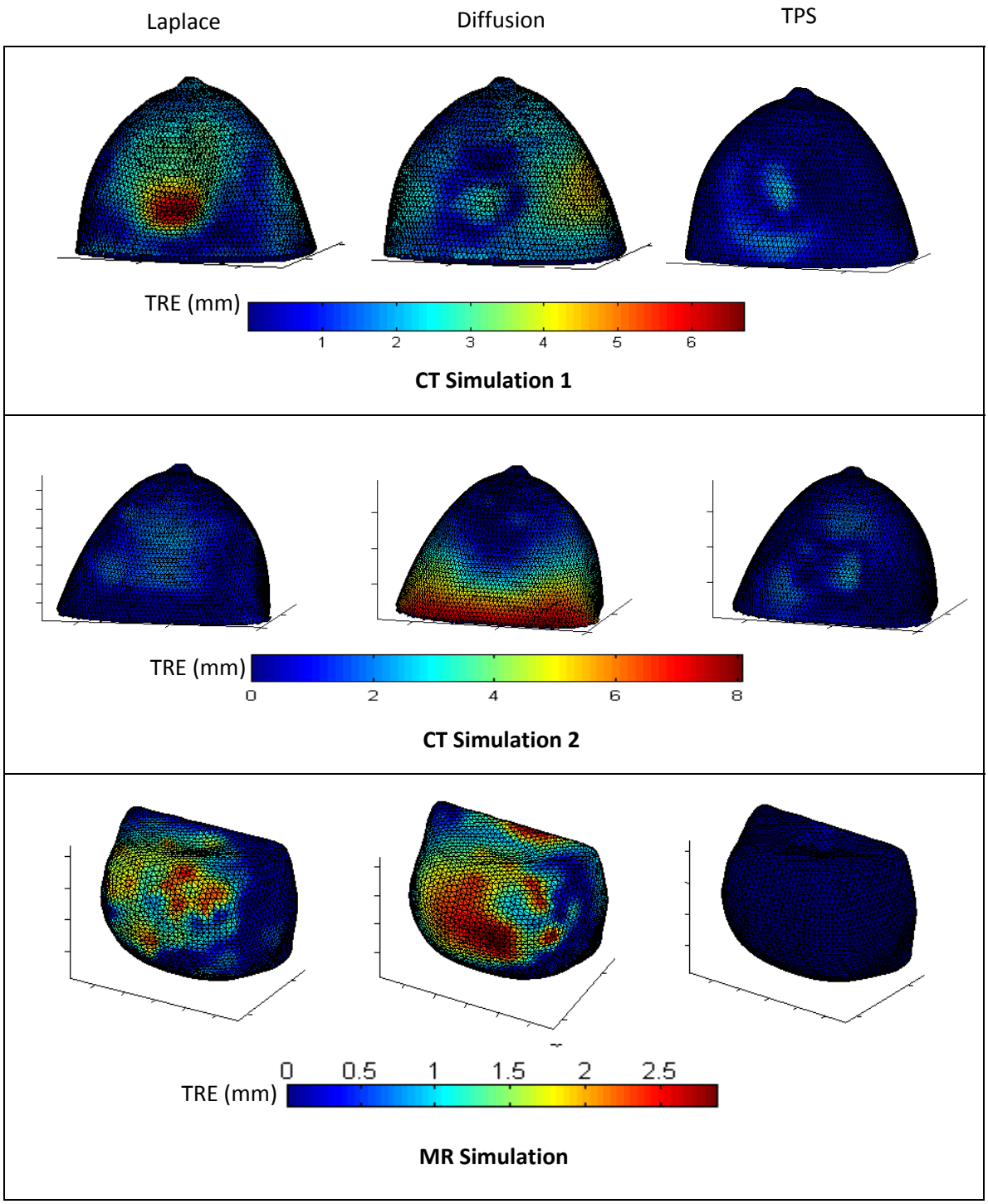

Figure 10. Error when breast surfaces deformed by three simulations were registered using the Laplace (left column), diffusion (middle column), and TPS (right column) registrations. The TPS registration method had lower error than the Laplace or diffusion methods in all three simulations.

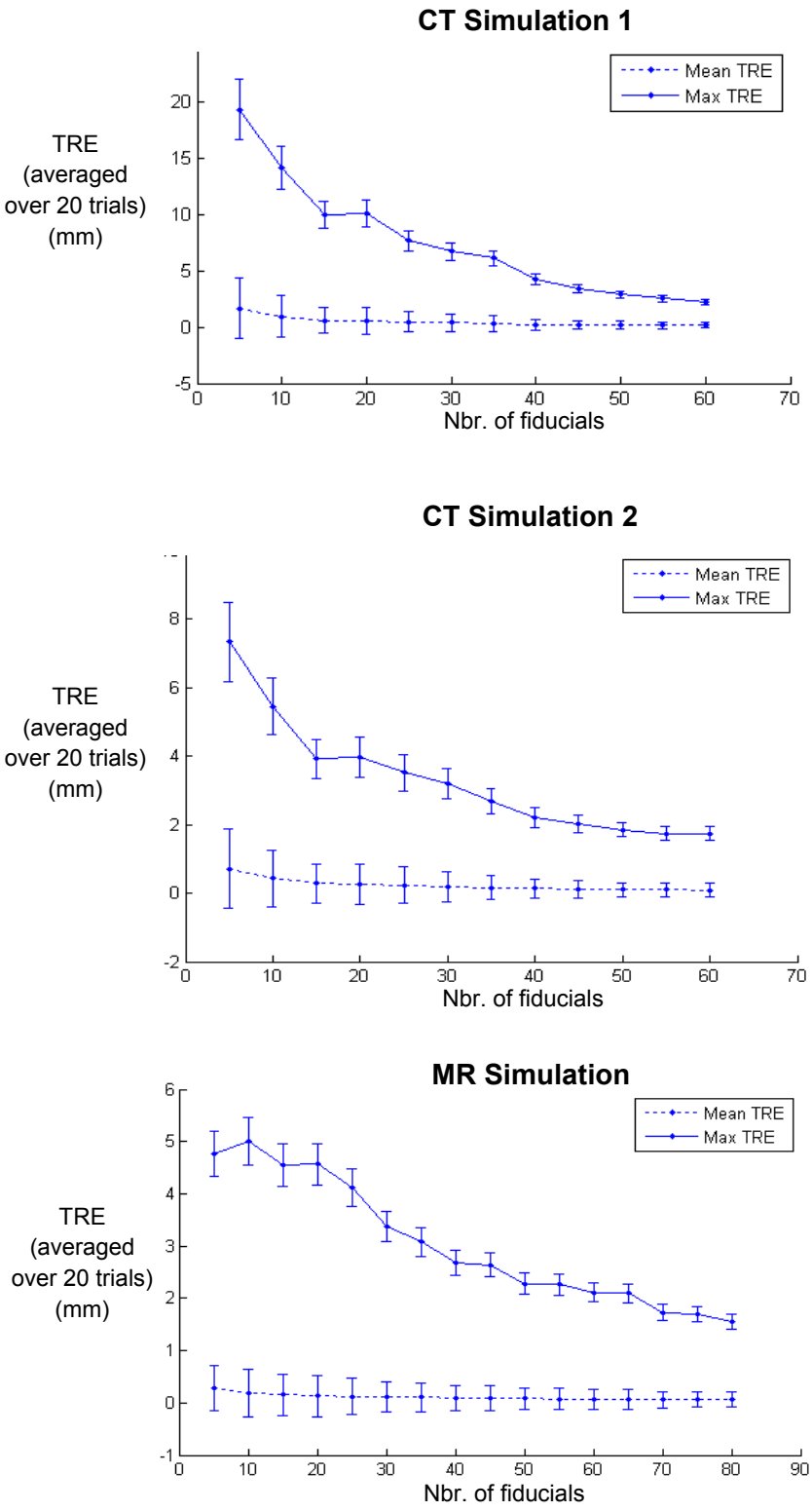

Figure 11. TPS registration error (averaged over 20 trials) for breast surfaces deformed by three simulations. Max and mean TRE were calculated for different numbers of uniformly distributed fiducials. TPS registration error decreased as the number of fiducials increased when a uniform distribution of fiducials was used.

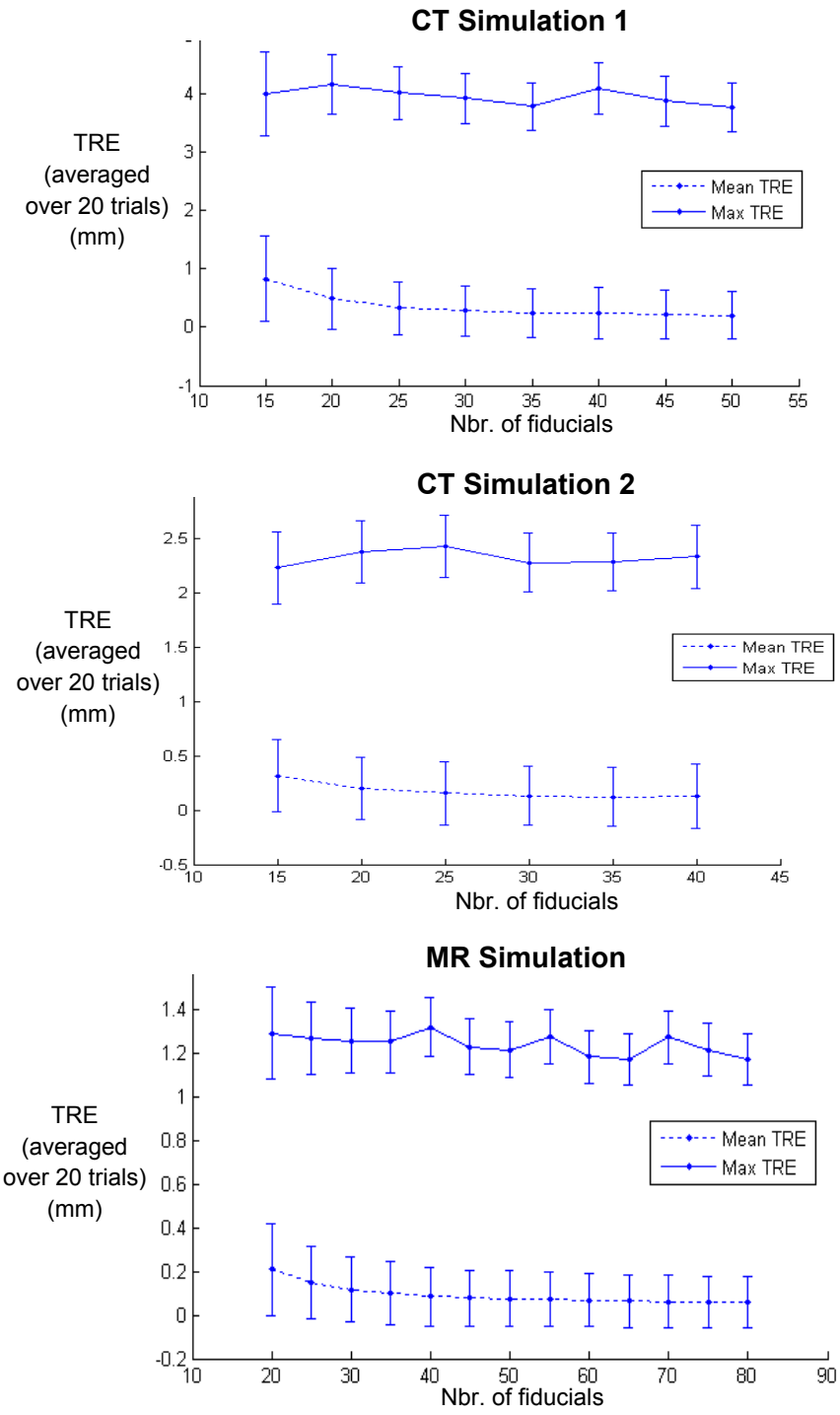

Figure 12. TPS registration error (averaged over 20 trials) for breast surfaces deformed by three simulations. Max and mean TRE were calculated for different numbers of non-uniformly distributed fiducials, where a high number of fiducials was placed in the region contacting the simulated compression bladder and a varying number elsewhere. When a high number of fiducials was placed in the contact region, increasing the number of total fiducials did not significantly decrease the TPS registration error.

Table 1. Max and mean TRE when the Laplace, diffusion, and TPS methods were used to register breast surfaces deformed by three simulations. The TPS registration method had lower TRE than the PDE-based methods for all three simulations.

	CT Simulation 1 (33 mm displacement)		CT Simulation 2 (13 mm displacement)		MR Simulation (6 mm displacement)	
	Max TRE (mm)	Max TRE (mm)	Max TRE (mm)	Mean TRE (mm)	Max TRE (mm)	Mean TRE (mm)
Laplace	8.5	1.6	2.6	0.5	2.5	0.5
Diffusion	6.7	1.8	8.0	1.5	2.9	0.6
TPS*	3.1	0.4	2.6	0.3	0.6	0.03

*TPS registration using 40 evenly distributed fiducials for CT simulations 1-2 and 60 for the MR simulation.

3.2 Phantom experiment

The Laplace and diffusion methods were used to determine point correspondence between the non-compressed and compressed surfaces of a breast phantom (Figure 13). The results were validated by calculating the TRE at 34 fiducials located directly below the surface of the phantom. For comparison, TPS was used to interpolate the displacements of 33 fiducials to all surface nodes, and the TRE was calculated using the remaining fiducial. The TPS registration was repeated using a different fiducial to calculate TRE each time, and the max and mean TRE were calculated.

The results for a 50 and 100% compression (with a maximum displacements of about 20 mm and 36 mm, respectively) are shown in Table 2. In contrast to the simulation experiment, the diffusion method performed slightly better than the Laplace method and had lower TRE. The TRE for the TPS registration using 33 fiducials for interpolation was lower than that for the PDE-based registrations.

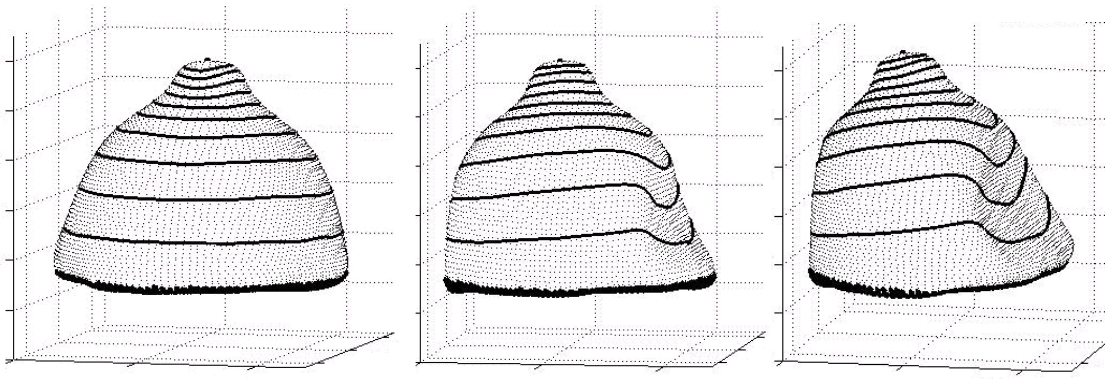

Figure 13. Breast phantom surface before compression (left), at 50% compression with maximum displacement of 20 mm (middle), and at 100% compression with maximum displacement of 36 mm (right). Lines indicate isocontours.

Table 2. Error for different registration methods tested on the breast phantom at 50% and 100% compression. (TPS registration was performed using 33 fiducials and 1 fiducial to calculate TRE. The TRE was averaged over 34 trials, where each trial used a different fiducial to calculated TRE.) The TPS method had lower TRE than the PDE-based methods for both phantom compressions.

	Phantom: 50% compression (20 mm displacement)		Phantom: 100% compression (36 mm displacement)	
	Max TRE (mm)	Mean TRE (mm)	Max TRE (mm)	Mean TRE (mm)
Laplace	8.6	3.4	15.3	6.3
Diffusion	6.8	2.7	13.6	5.7
TPS	3.4	1.1	5.1	1.7

3.3 Clinical data

In order to assess the feasibility of using the PDE-based registration methods in a clinical application, the Laplace and diffusion methods were used to register a clinical dataset before and after compression (Figure 14). A qualitative inspection of the displacement fields seem to indicate that both the Laplace and diffusion registrations yield reasonable results.

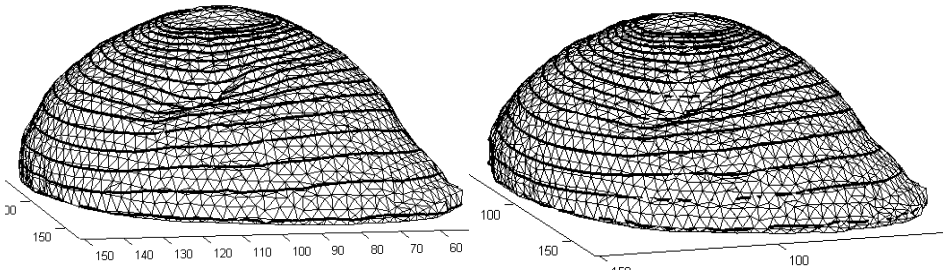

Figure 14: Clinical source (left) and target (right) meshes, displayed with Laplace solution isocontours. (Axes units in mm.)

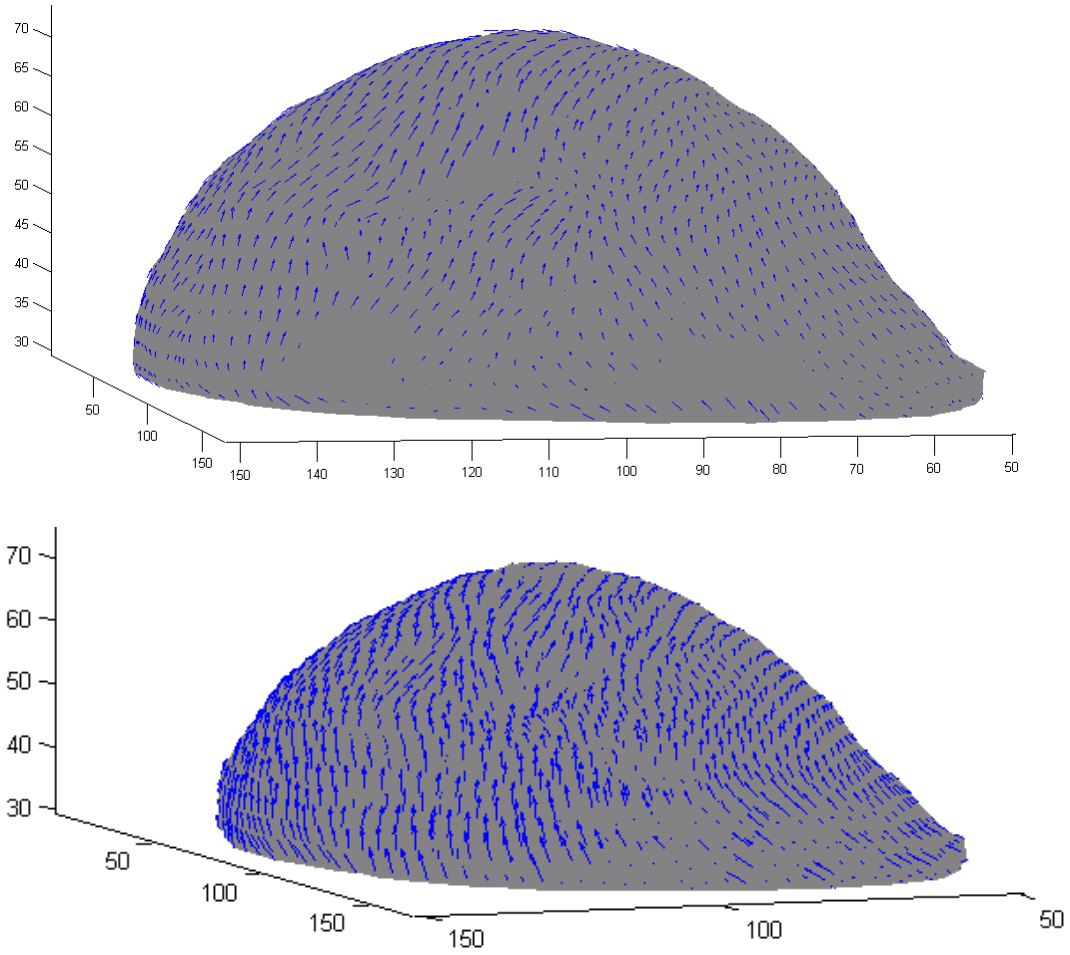

Figure 15: Clinical source surface displayed with displacement field determined by Laplace (top) and diffusion (bottom) registration. (Axes units in mm.)

3.4 MIE reconstruction

MIE elasticity reconstructions were performed on the breast surface deformed by CT simulation 1 using boundary conditions from the Laplace, diffusion, and TPS registrations in order to assess the reconstruction accuracy using each registration method. The ratios of tumor to surrounding tissue elasticity were reconstructed given a simulated tumor with elasticity six times more stiff than the surrounding homogenous tissue. The results of these reconstructions (Table 3) show that the registration methods with lower TRE, i.e. the registration methods that are more accurate, result in more accurate elasticity reconstructions.

Table 3. Ratio of the tumor to surrounding tissue elasticity reconstructed by MIE when boundary conditions from Laplace, diffusion, and TPS registrations are used. The accuracy of MIE reconstruction can be assessed by comparing the reconstructed elasticity contrast ratio to the simulated contrast ratio of 6.0. The mean TRE of the registration method has been included for comparison. The registration methods with lower TRE resulted in more accurate MIE elasticity reconstructions.

	CT Simulation 1	
	Reconstructed elasticity contrast ratio	Mean TRE (mm)
Diffusion	17.5	1.5
Laplace	5.02	0.52
TPS	5.66	0.26

CHAPTER 4

DISCUSSION

Of the three registration methods evaluated, the TPS method given a sufficient number of fiducials consistently outperformed the Laplace and diffusion methods and had the lowest error for both the simulation and phantom experiments. However, it is important to note that a comparison of the PDE-based methods and the TPS method is not entirely fair since the TPS method relies on fiducial information that the Laplace and diffusion methods do not require.

The accuracy of the TPS registration is dependent on both the number and placement of the fiducials. When a uniform fiducial distribution is used, the error decreases as the number of fiducials is increased; however, the error reduction becomes insignificant when the number of fiducials is increased beyond a certain number. When a non-uniform fiducial distribution is used, in which the density of fiducials is higher in the deformed region than elsewhere, the same amount of error can be achieved using fewer fiducials. In the case of the simulation data, when a uniform fiducials distribution was used, about 40 fiducials was required to lower the maximum error below 3 mm. When more fiducials were placed in the region in contact with the simulated compression bladder, however, the number of fiducials required to obtain the same about of error was approximately cut in half.

The results indicate that although the Laplace method did not perform as accurately as the TPS method, it still may be a usable surface registration method, especially if fiducials are not available. However, one of the challenges of the Laplace method is determining the regions to which boundary conditions are assigned. Accurate selection of these regions is important because the implicit correspondence between these regions is used by the Laplace equation to obtain the correspondence for the rest of the surface. For these studies, the nipple region and the chest wall boundary regions were selected manually. Further studies may be needed to find a method to automate the selection of the boundary regions and to evaluate how error in the selection of these regions affects the final registration error.

The diffusion method performed better than the Laplace method in some cases and worse in others. The disadvantages of the diffusion method are that several parameters (the time step and final time) must be manually fine-tuned to optimize performance. Since the diffusion described by the PDE is by definition a non steady-state process, an optimal registration requires that the diffusion front should travel over the entire surface between the nipple and base and stop at the base in order to assure correspondence for as much as the surface as possible. If the parameters are chosen such that the diffusion front does not reach the base, the correspondence for the regions not reached by the diffusion front cannot be constrained and must be interpolated from the displacements of the surrounding regions. Conversely, if the diffusion front travels for too long a time, the solution over the surface approaches saturation, resulting in a flat gradient and lack of isocontours from which to establish correspondence. Various modifications to the diffusion method employing curvature information and using different diffusion coefficients were tested, but none was very successful.

However, the diffusion method does have some advantages over the Laplace and TPS methods. Careful selection of the parameters can enable the diffusion method to outperform the Laplace method for some datasets. In fact, one possible improvement to this method could be to incorporate an optimization scheme that chooses the ideal diffusion parameters to minimize an image similarity measure. Another advantage of the diffusion method is that it only requires boundary conditions to be set in one region (in this case, the nipple), unlike the Laplace method, which requires boundary conditions at two regions (nipple and chest wall base), and the TPS method, which requires multiple points of constraint (at 34 fiducials).

In general, the TRE measured for each registration technique is not only dependent on the factors described above, but also on the amount of deformation of the target surface. Using the simulation and phantom data presented here, one may be able to estimate the range of error expected when one of the described methods is used to register breast surfaces with a particular amount of compression. Conversely, the maximum amount of compression that will yield a registration within a given error bound can be roughly estimated. For the purposes of MIE, realistic compressions will be in the range of 1-2 cm.

Another factor related to the amount of compression is the distribution of TRE over the surface. The TRE was not evenly distributed; rather, the TRE in the areas of greatest deformation tended to be higher than the TRE elsewhere. Therefore, the mean TRE is not necessarily the best measure of the TRE over the surface; the max TRE may reflect the error in the deformed regions more accurately.

In comparison to previous studies, the Laplace method outperformed the modified SCP method implemented by Schuler, et al. The data generated by CT simulation 2 was also used to test the modified SCP method, and whereas the Laplace method had a maximum error of 8.5 mm for a deformation of 33 mm, the modified SCP method had a maximum error of 27.8 mm (Schuler, 2006). Direct comparisons with Tanner's study (2007) are not entirely possible because the data and biomechanical models differ. However, the results of CT simulation 2 and the MR simulation are probably the most comparable because the maximum amount of deformation (13 mm and 6 mm, respectively) is within the range described in Tanner's study (0-17 mm). The TRE reported in Tanner's study (mean: approximately 0.5-0.9mm, max: approximately 3-6mm) seems comparable to that of the Laplace registration for CT simulation 2 and the MR simulation (mean: 0.48-0.52 mm, max: 2.5-2.6 mm). These results seem to tentatively indicate that performance of the registration methods from the two studies is comparable. As Tanner's study does not include deformations greater than about 17 mm, the results of the phantom registrations cannot be compared. However, one advantage of the PDE-based methods over Tanner's method is that the PDE-based methods do not require an optimization based on image similarity and are therefore probably less computationally expensive and avoid entrapment in local minima.

MIE is one application that may use the registration methods described in this paper, in this case to determine boundary conditions for its elasticity model. The results for the simulation data set indicate that the most accurate reconstruction was obtained using boundary conditions from the registration method with the lowest TRE. In this case, the TPS method resulted in the most accurate reconstruction, followed by the Laplace method, which also resulted in a fairly accurate reconstruction. These preliminary studies seem to indicate that the TPS method should be the registration method of choice if a sufficient number of fiducials are available. However,

depending on the amount of registration error, the Laplace or diffusion methods may result in fairly accurate reconstructions if fiducials are not available.

CHAPTER 5

CONCLUSION

The results of the simulation and phantom experiments indicate that while TPS interpolation is the most accurate surface registration method of those evaluated, the Laplace and diffusion methods may be viable surface registration techniques if fiducials are not available. Although the TPS method was consistently more accurate than the PDE-based methods, its accuracy is dependent on the number and distribution of fiducials available. While the Laplace method generally provides a more accurate and reliable registration, in some cases the parameters of the diffusion method can be fine-tuned so as to provide a more accurate registration than the Laplace method. When the results of the registration methods are used to specify boundary conditions in MIE elasticity reconstructions, the TPS method results in the most accurate reconstructions, probably because it is the most accurate registration method. However, depending on the amount of registration error, the PDE-based registration methods may also be usable in MIE elasticity reconstructions. In addition to MIE, the Laplace and TPS methods also have potential to be used for non-rigid registration of breast surfaces in other breast imaging applications.

REFERENCES

American Cancer Society. (2007). Cancer Facts and Figures 2007. Retrieved Jan 18, 2007, from http://www.cancer.org/downloads/STT/CAFF2007PWSecured.pdf.

Bayford, R. H. (2006). Bioimpedance tomography (Electrical impedance tomography). *Annual Review of Biomedical Engineering, 8*, 63-91.

Besl, P. J. & McKay, N. D. (1992). A method for registration of 3-D shapes. *IEEE Trans. on Pattern Analysis and Machine Intelligence, 14*(2):239-256.

Brooksby, B. A., Dehghani, H., Pogue, B. W., & Paulsen, K. D. (2003) . Near-infrared (NIR) tomography breast image reconstruction with a priori structural information from MRI: algorithm development for reconstructing heterogeneities. *IEEE Journal of Selected Topics in Quantum Electronics*, 9: 199-209.

Chui, H. L. & Rangarajan, A. (2003). A new point matching algorithm for non-rigid registration. *Computer Vision and Image Understanding*, *89*(2-3): 114-141.

Crum, W. R., Tanner, C., et al. (2005). Anisotropic multi-scale fluid registration: evaluation in magnetic resonance breast imaging. *Physics in Medicine and Biology, 50*(21): 5153-5174.

Davis, M. H. & Khotanzad, A., et al. (1997). A physics-based coordinate transformation for 3-D image matching. *IEEE Transactions on Medical Imaging 16*(3): 317-328.

Dinh, H. Q. (2002). Implicit Shapes: Reconstruction and Explicit Transformation. PhD Dissertation, Georgia Institute of Technology.

Froh, M. S., Barber, D. C., et al. (2006). Piecewise-quadrilateral registration by optical flow - Applications in contrast-enhanced MR imaging of the breast. *Medical Image Computing and Computer-Assisted Intervention - Miccai 2006, Pt 2*, *4191*: 686-693.

Goshtasby, A. (1988). Registration of Images with Geometric Distortions. *IEEE Transactions on Geoscience and Remote Sensing, 26*(1): 60-64.

Greenleaf, J.F., Fatemi, M., & Insana, M. (2003). Selected methods for imaging elastic properties of biological tissues. *Annual Review of Biomedical Engineering*, 5: 57-78.

Guo, Y. J., Sivaramakrishna, R., et al. (2006). Breast image registration techniques: a survey. *Medical & Biological Engineering & Computing, 44*(1-2): 15-26.

Hajnal, J. V., Hill, D. L. G., Hawkes, D. J. (2001). *Medical Image Registration*. New York: CRC Press LLC.

Miga, M. I. (2003). A new approach to elastography using mutual information and finite elements, *Physics in Medicine and Biology*, 48, 467-80.

Papademetris, X., Sinusas, A. J., et al. (2002). Estimation of 3-D left ventricular deformation from medical images using biomechanical models. *IEEE Transactions on Medical Imaging, 21*(7): 786-800.

Pellot-Barakat, C., Sridhar, M., Lindfors, K. K., & Insana, M. F. (2006). Ultrasonic elasticity imaging as a tool for breast cancer diagnosis and research. *Current Medical Imaging Reviews, 2*(1), 157-164.

Rohlfing, T., Maurer, C. R., et al. (2003). Volume-preserving nonrigid registration of MR breast images using free-form deformation with an incompressibility constraint. *IEEE Transactions on Medical Imaging, 22*(6): 730-741.

Roose, L., Mollemans, W., et al. (2006). Biomechanically based elastic breast registration using mass tensor simulation. *Medical Image Computing and Computer-Assisted Intervention - Miccai 2006, Pt 2, 4191*: 718-725.

Rueckert, D., Hayes, C., et al. (1998). Non-rigid registration of breast MR images using mutual information. *Medical Image Computing and Computer-Assisted Intervention – Miccai 1998. 1496*: 1144-1152.

Rueckert, D., Sonoda, L. I., et al. (1999). Nonrigid registration using free-form deformations: Application to breast MR images. *IEEE Transactions on Medical Imaging, 18*(8): 712-721.

Schuler, D. R., Ou, J. J., Barnes, S. L., Miga, M. I. (2006) Automatic surface correspondence methods for a deformed breast. *Proceedings of SPIE, Medical Imaging 2006.*

Tanner, C., Schnabel, J. A., et al. (2007). Quantitative evaluation of free-form deformation registration for dynamic contrast-enhanced MR mammography. *Medical Physics, 34*(4): 1221-1233.

Tanner, C., Schnabel, J. A., et al. (2006). Factors influencing the accuracy of biomechanical breast models. *Medical Physics, 33*(6): 1758-1769.

Thirion, J. P. (1996). New feature points based on geometric invariants for 3D image registration. *International Journal of Computer Vision, 18*(2): 121-137.

Washington, C. W. & Miga, M. (2004). Modality independent elastography (MIE): a new approach to elasticity imaging. *IEEE Transactions on Medical Imaging*, 23, 1117-28.